Marine and Petroleum Geology 171 (2025) 107142

Contents lists available at ScienceDirect

Marine and Petroleum Geology

journal homepage: www.elsevier.com/locate/marpetgeo

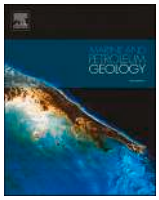

Tectonics of cauvery basin (India) in onshore and offshore portions

Soumyajit Mukherjee [a,*], Kutubuddin Ansari [b], Adrija Raha [c], Mery Biswas [c], Subhobroto Mazumder [d]

[a] Department of Earth Sciences, Indian Institute of Technology Bombay Powai, Mumbai, 400 076, Maharashtra, India
[b] Integrated Geoinformation (IntGeo) Solution Private Limited, New Delhi, 110 025, India
[c] Department of Geography, Presidency University, Kolkata, West Bengal, 700 073, India
[d] Oil and Natural Gas Corporation, NBP Green Heights, C-69, Bandra Kurla Complex Road, G Block BKC, Bandra East, Mumbai, Maharashtra, 400 051, India

ARTICLE INFO

Keywords:
Extensional tectonics
Coastal tectonics
Indian plate
Geodynamics
Structural geology

ABSTRACT

Morphometric studies coupled with geophysical investigations from petroliferous basins provide valuable information about tectonics of the regions. We deduce six morphologic parameters from the River Cauvery's designated (sub)watersheds and perform dendrogram clustering analysis. The main channels of the (sub)watersheds showcase steeper gradient and meandering nature with less concavity. On the other hand, the distributaries portray lesser gradient and straight nature with greater concavity. From the offshore region of the Cauvery basin, we perform gravity modeling. The results show variations in gravity values from low to high, −150 to 50 mGal probably because of the basement ridge-depression features. This anomaly orientation indicates the extension of the sub-basin in the region. A strong NE-SW gravity trend possibly suggests a high-density plug at crustal-level. The low gravity values near the Vedaranyam region indicate low-density rocks within the basement. Places of high gravity anomaly show a decrease in bathymetry depth and vice versa. This indicates isostatic compensation of the Moho geometry, possibly due to crustal thinning in the offshore areas. Isostatic regional gravity fields are manifested by Moho relief and can have implications on the lithospheric mechanical strengths. Bathymetric studies indicate multi-directional slopes. Relatively flat areas can indicate depocenters. E-W trending lineaments mapped on the Precambrian basement from a portion of the study area is presumably a manifestation of Cauvery Shear zone, which also persists in the offshore region.

1. Introduction

Petroliferous basins' morphometry and geophysical information are of tremendous importance from the exploration perspectives (reviews in Zou, 2017; Saha, 2022). Combined seismicity and geomorphic studies have bene proved fruitful by other research groups from different places in the world (e.g., Pasari et al., 2021; Andrean et al., 2023; Simanjuntak et al., 2024). The Cauvery basin, variously referred as a failed rift and a pericratonic rift basin, located at the southern part of the eastern Indian margin is a Category I basin with established production. The basin is located along the Eastern Continental Margin of India (ECMI) as a major pericratonic rift basin. Recently the basin has been studies for basement production issues (Mazumder et al., 2019).

Morphometric studies from onland areas can demarcate subzones of higher tectonic activity within a watershed (e.g., Mondal et al., 2023). Combining such works with the geophysical data set, the geoscientist can comment about the tectonics of the terrain. Such works become crucial when performed from coastal areas of hydrocarbon prospect (e.g., Dasgupta et al., 2022).

Bathymetry in a broad sense means submarine topography. Bathymetric maps show the land that is underwater, much as topographic maps represent relief in 3D of the overland terrain. Depth contours/isobaths are lines representing same depths below the water surface. With the first launch of the Seasat mission in 1978 in USA, remotely measuring sea surface height undulations caused by the gravimetric method effects of underwater topography with satellite-based timers began (Born et al., 1979). The development of multi-beam echo sounders in recent decades has greatly improved the efficiency, accuracy and spatial resolution of mapping the shoreline and ocean. Satellite altimetry measurements can generate bathymetry (Hell, 2011 and references therein). Digital Bathymetric Model (DBM) is usually found out for relatively smaller areas (e.g. Klenke and Schenke, 2002; Hell, 2011). Bathymetric data help to assess the slope direction of the undulating terrain and topographic slope determine the deposition pattern in

* Corresponding author.
E-mail addresses: smukherjee@iitb.ac.in, soumyajitm@gmail.com (S. Mukherjee).

https://doi.org/10.1016/j.marpetgeo.2024.107142
Received 24 August 2024; Received in revised form 30 September 2024; Accepted 1 October 2024
Available online 4 October 2024

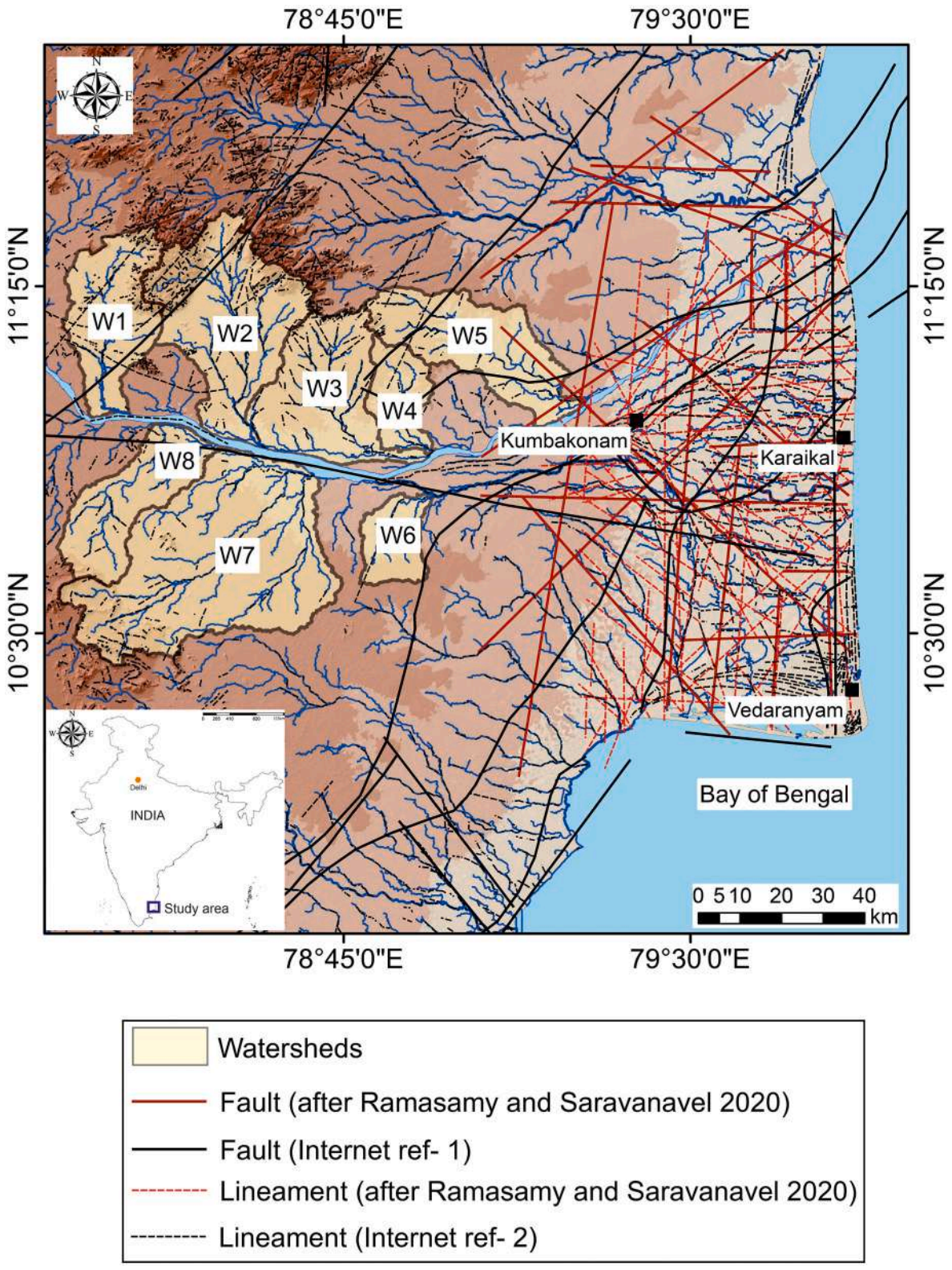

Fig. 1. Eight delineated sub-watersheds of lower Cauvery overlain with the lineaments and faults.

marine depressions and ridges.

This work aims at *(i)* Understanding the tectonic imprint on the sub-watersheds and channels specifically from the southern portion of the Cauvery basin in the onland area, *(ii)* understanding the effect of gravity on uncompensated bathymetry topographic depth for the Cauvery basin, and *(iii)* specifying the offshore topographic slope direction and slope ranges with contour spacing from the coastline to the sea.

Table 1
Definitions, explanations and obtained magnitudes for basin-scale morphometric parameters. W: Watershed.

Sl. No.	Morphometric parameters	Equations	Explanations	Obtained magnitudes	Reference
1	**Asymmetry factor** (AF)	$AF = \left(\frac{A_r}{A_t}\right)*100$ A_r: area of the basin (km^2) to the right of the main channel facing downstream and A_t: total area (km^2) of the basin.	An indication of the degree of tectonic tilt in a river basin. The main stream shifts due to tectonic activity, sloping away from the midline of the basin.	W1 = 0.252 W2 = 8.484 W3 = 10.567 W4 = 1.842 W5 = 5.233 W6 = 15.562 W7 = 3.132 W8 = 14.711	Hare and Gardner (1985); e.g. Anand and Pradhan (2019)
2.	**Elongation Ratio** (R_e)	$Re = 1.128\sqrt{\frac{A}{L_b}}$ A: signifies the area of the basin, Lb: denotes the length of the basin.	Elongation ratio is influenced by geology and climate. The values vary from 0 to 1 (e.g. Wołosiewicz, 2018). As the landscape evolves, the river basin becomes circular and the value tends to be 1.	W1 = 0.626 W2 = 0.712 W3 = 0.852 W4 = 0.647 W5 = 0.579 W6 = 0.701 W7 = 0.749 W8 = 0.598	Schumm (1956); e.g. Wołosiewicz (2018)
3.	**Circularity Ratio** (Rc)	$Rc = \frac{4\pi A}{P^2}$ Where, P: indicates the perimeter of river basin. A: signifies the area of the basin.	The climate, slope, length and frequency of streams, and geological formations all affect the river basin's circularity ratio. Elevated values signify the basin's circular geometry and, as a result, the advanced phase of landscape development.	W1 = 0.330 W2 = 0.320 W3 = 0.340 W4 = 0.383 W5 = 0.284 W6 = 0.383 W7 = 0.360 W8 = 0.321	Horton (1945)
4.	**Basin shape index** (Bs)	$Bs = \frac{Bl}{Bw}$ Bl: measured length from headwater to the point on the mouth of the basin, Bw: measured width at the widest point on the basin	In the tectonically active area, the basin tends to be elongated.	W1 = 2.683 W2 = 1.396 W3 = 1.624 W4 = 1.948 W5 = 2.912 W6 = 1.933 W7 = 1.872 W8 = 3.429	E.g. Ramírez-Herrera (1998); Bull and McFadden (1977); Anand and Pradhan (2019)
5.	**Transverse topographic symmetry factor** (T)	$T = \frac{Da}{Dd}$ The ratio between the distance from the drainage basin's midline to the meander belt's midline (Da) and the distance from the basin's midline to the basin divide (Dd) is known as the transverse topographic symmetry factor.	In a fully symmetric basin, transverse topographic symmetry (T) is zero. As asymmetry arises, T also increases and eventually reaches a value of one. The transverse topographic symmetry factor is calculated for different stream channel lengths and indicates the preferred migration path of the stream, which is perpendicular to the drainage axis.	W1 = 0.180 W2 = 0.220 W3 = 0.420 W4 = 0.250 W5 = 0.490 W6 = 0.830 W7 = 0.150 W8 = 0.660	Cox (1994) E.g. Raha et al. (2023)
6.	**Drainage texture** (D_t)	$D_t = Nu/P$ Nu: Number of streams of a given order. P: Perimeter (km) of the watershed	The drainage texture is influenced by the relief features, underlying lithology, and infiltration capacity of the terrain. According to Horton (1945), Dt is the total number of stream segments along the watershed's margin in all orders. The relative channel spacing in dynamically prepared terrain is determined by a variety of natural elements, including the kind of soil and rock, the amount of precipitation, vegetation, permeability, undulations, and the stage of watershed development (Kale and Gupta, 2001).	W1 = 0.861 W2 = 0.567 W3 = 0.544 W4 = 0.304 W5 = 0.593 W6 = 0.394 W7 = 0.874 W8 = 0.488	Cox (1994)

Table 2
Proximity matrix based on squared Euclidian distance.

Proximity Matrix								
Case	Squared Euclidean distance							
	1	2	3	4	5	6	7	8
1	0.000	69.517	107.729	3.387	25.035	235.607	8.968	209.990
2	69.517	0.000	4.451	44.499	12.960	50.792	28.973	43.120
3	107.729	4.451	0.000	76.361	30.197	25.261	55.533	20.557
4	3.387	44.499	76.361	0.000	12.584	188.586	2.015	168.012
5	25.035	12.960	30.197	12.584	0.000	107.827	5.724	90.141
6	235.607	50.792	25.261	188.586	107.827	0.000	155.204	3.014
7	8.968	28.973	55.533	2.015	5.724	155.204	0.000	136.928
8	209.990	43.120	20.557	168.012	90.141	3.014	136.928	0.000

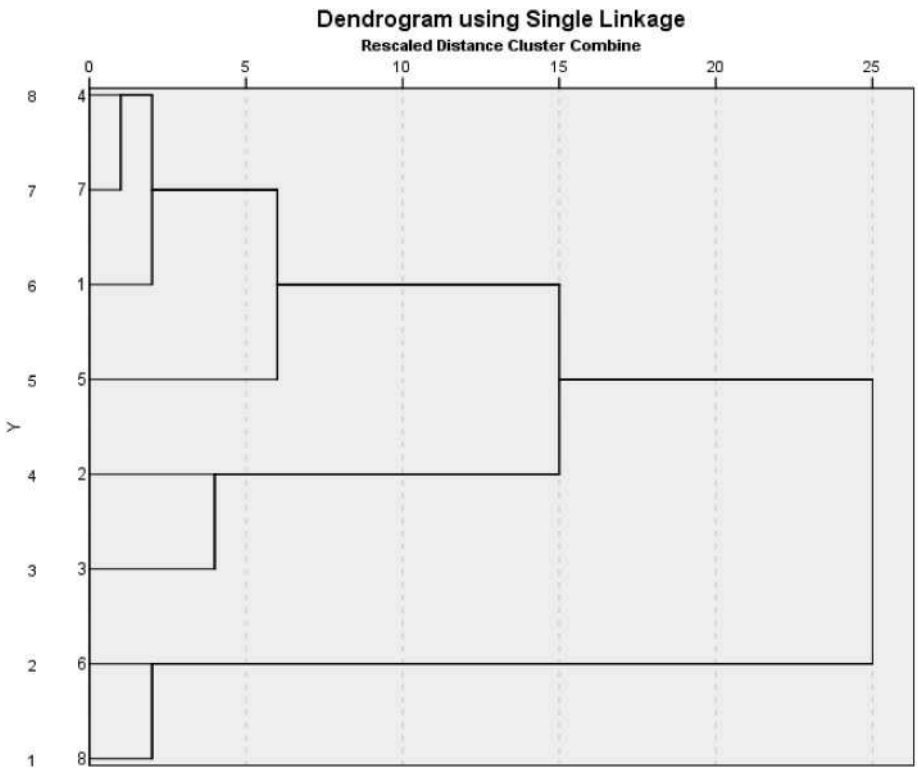

Fig. 2. Dendrogram showing the clusters of eight sub-watersheds based on selected areal and relief parameters.

2. Present research

2.1. Geoscience of study area

We study the onshore and offshore portions of Cauvery basin (Fig. 1). The Cauvery basin has a history of poly-phase rift-drift transition (review in Dasgupta, 2019). Late-Jurassic – Early Cretaceous rifting of the Indian plates ascribed for the genesis of this basin (Bastia and Radhakrishna, 2012). The basin was actually a part of a larger rift system involving the Palar-Pennar, Krishna-Godavari and Mahanadi rift zones (review in Dasgupta et al., 2022). The southern part of Cauvery basin developed related to the India-Sri Lanka separation (review in Biswas et al. et al., submitted). Dextral and oblique slip along the Coromondal Transform margin defines the end of the decipherable development of this basin (review in Dasgupta, 2019). The Cauvery Shear Zone is an important mega-scale structure that was activated in the Neoproterozic Period (Chetty and Rao, 2006). Relay structures, transform zones, shallow detachment and polygonal faults, are few important first order structures of this basin in the offshore region (Dasgupta, 2018, Dasgupta et al., 2022; Dasgupta and Maitra, 2018; Dasgupta and Misra, 2018; Misra and Dasgupta, 2018a,b). The deep offshore morphology in this basin is categorized by very steep continental slope, which differs significantly from the other parts of the ECMI (Twinkle et al., 2014).

Mitra and Agarwal (1991) based on lineament studies on remote sensing images deciphered that the northern part of the Cauvery onshore basin is more active neotectonically than the southern part. A similar conclusion is reached by Sharma and Rajamani (2000) based on geochemical studies. Ramasamy et al. (2011) documented through remote sensing studies that N-S, E-W and NE-SW trending lineaments in the Cauvery onland area are tectonically active. Marine geohazards such as the slope-instability has been noticed from the offshore Cauvery basin (Bastia et al., 2011). Recent geophysical studies from this basin indicates dense fracture network at depth (Mogali et al., 2024) including the basement granites (Deepa et al., 2019). Ramkumar et al. (2019) documented few rivers in the Cauvery onshore area are tectonically active (also see Ramasamy and Saravanavel, 2020). Recent geophysical studies from the Cauvery basin indicates that the basin has NE-SW trending linear gravity high bands, two (sub)circular gravity lows and E-W linear structures (Ganguli and Pal, 2023).

2.2. Geomorphic input

2.2.1. Morphometric parameters

Eight sub-watersheds are delineated along the lower Cauvery River through ArcGIS 10.4 (2016). Six morphometric parameters have been deduced from these (sub)watersheds (Table 1).

2.2.2. Clustering

Hierarchical clustering is carried out based on the same indicators in the (sub)watershed scale. Each segment was compared to its neighbours using the Euclidean-based dissimilarity method (Ward, 1963; Eisen et al., 1998) to assess how similar they were. Clustering works on unsupervised classification and can discriminate signals (grouping signals) from noise (source signals).

2.2.3. Linear parameters

Three selected linear parameters (Table 2) are obtained on the master streams of the selected (sub)watersheds and on the main distributaries of the delta region.

2.3. Geophysical input

The analytical expression of effect of gravity on uncompensated bathymetry topographic depths for a terrain is given by (Parker, 1973):

$$\Delta g_{bathymetry}(k) = 2\pi G(\rho_m - \rho_c)e^{-kd}\sum_{n=1}^{\infty}\frac{k^{n-1}}{n!}F\{h^n(x,y)\} \quad \text{(eqn 1)}$$

here ρ_m and ρ_c are the densities of the mantle and the crust, respectively, in gm cm^{-3}. The gravitational constant is indicated by G (m^3 kg^{-1} s^{-2}) and an undulating bathymetry Fourier transform by F{h(k). Further, d is

Table 3
Definitions, explanations and obtained magnitudes for linear morphometric parameters. W: Watershed.

Sl. No.	Linear scale indicators:	Equations	Obtained magnitude [R1-8 = Main streams of selected sub-watersheds; D1-11 = Distributaries]	References
1	Stream –length Gradient index (SL)	$SL = \frac{h_1 - h_2}{[\ln(d_2) - \ln(d_1)]}$ Where, 'h_1' and 'h_2' represent height of the first and second point from the source respectively. 'd_1' and 'd_2' represents the distance of first and second point from the source respectively. Higher SL values specify the crossing points of major faults and lineaments both in across and along and lower the values Denote fractures and small-scale lineaments.	R1 = 19.059 R2 = 15.953 R3 = 8.310 R4 = 5.647 R5 = 9.350 R6 = 4.244 R7 = 20.517 R8 = 12.873 D1 = 0.734 D2 = 5.59 D3 = 1.374 D4 = 2.178 D5 = 2.66 D6 = 1.539 D7 = 5.496 D8 = 1.308 D9 = 1.041 D10 = 0.885 D11 = 6.152	Hack (1957); e.g. Seeber and Gornitz (1983); Bishop et al. (1985); Goldrick& Bishop (1995); Goldrick and Bishop (2007); Lee and Tsai (2009); Biswas et al. (2022b).
3	Sinuosity Index (SI)	$SI = \frac{CL}{Vl}$ Where, CL: channel length between two points on a river and Vl: valley length.	R1 = 1.63 R2 = 1.26 R3 = 1.55 R4 = 1.43 R5 = 1.45 R6 = 1.53 R7 = 1.32 R8 = 1.84 D1 = 1.75 D2 = 1.23 D3 = 1.55 D4 = 1.61 D5 = 1.34 D6 = 1.52 D7 = 1.22 D8 = 1.51 D9 = 1.58 D10 = 1.72 D11 = 2.69	Leopold and Wolman (1960)
4	Channel concavity (ɵ)	$S = ksA^{-\theta}$ S: channel slope; ks: is a steepness index, and 'a' is the concavity index. Channel concavity explain the differential rates of uplift and erosion. The concept was developed as a relationship between slope and area. Whipple (2004) has categorized concavity (ɵ) into four types: i) Low concavity (<0.4) is related to short, steep drainage dominated by debris flow, ii) Moderate concavity (0.4–0.7) is associated with actively uplifting bedrock channel, iii) High concavity (0.7–1) is related to decrease in the uplift and iv) Extremely high concavity (>1) denotes a transition from incisive to depositional conditions.	R1 = 0.215 R2 = 0.256 R3 = 0.236 R4 = 0.170 R5 = 0.351 R6 = 0.127 R7 = 0.353 R8 = 0.252 D1 = 0.389 D2 = 0.724 D3 = 0.374 D4 = 0.579 D5 = 0.471 D6 = 0.409 D7 = 0.651 D8 = 0.534 D9 = 0.509 D10 = 1.178 D11 = 1.320	Hack (1957); e.g. Lee and Tsai (2009)

the mean mantle depth (in km) and k the wave number in km^{-1}. Here n stands for the order of the equation. Putting n = 1 in eqn (1), we get the first-order expression of the analytical solution (Watts, 2001).

$$\Delta g_{bathymetry}(k) = 2\pi G(\rho_m - \rho_c)e^{-kd}F\{h(x,y)\} \quad \text{(eqn 2)}$$

here it is assumed that in eqn (2) that bathymetry is linearly connected with gravity anomaly in the wave number domain.

To analyze the local isostatic study, we used the Airy-Heiskanen model in which the local isostatic compensation of surface topography was compensated at the Moho. This was performed by using the following formula (Kumar et al., 2011; Ganguli and Pal, 2023):

$$\omega(x,y) = H(x,y) + \left[\frac{h(x,y).\rho_c}{\rho_m - \rho_c}\right] \quad \text{(eqn 3)}$$

here w(x,y) is the interface of crust and mantle (local isostatic compensation of surface topography). The reference depth and elevation of particular location are given by H(x,y) and h(x,y), respectively.

2.4. Bathymetry

Bathymetric data were downloaded from internet ref-3 within the domain of 78°E– 83°E and 7°E-13°E. This 3D data is processed in Arc GIS 10.8.1 (2020) platform. The data set is based on General Bathymetric Chart of the Oceans (GEBCO's) global bathymetric grids developed since 2019, through The Nippon Foundation-GEBCO Seabed 2030 Project. It is a collaboration between the Nippon Foundation (Japan) and the GEBCO. In April 2023, the GEBCO_2023 Grid was made available. It offers elevation data in meters for the entire world in a grid with 15 arc-second intervals. With 43200 rows and 86400 columns, it has 3,732, 480,000 data points worldwide. The elevations in meters at the centre of grid cells are referenced by the data values, which are pixel-centre registered (Internet ref-4). Toolbox plugin is used to find the slope direction and the amount. Contours of 50 m spacing generated from the 3D data gives the continental shelf to slope pattern.

3. Results

3.1. Geomorphology aspect

3.1.1. Morphometric parameters

The values of AF indicate the varying degrees of asymmetry present in the sub-watersheds of the lower Cauvery River. The highest amount

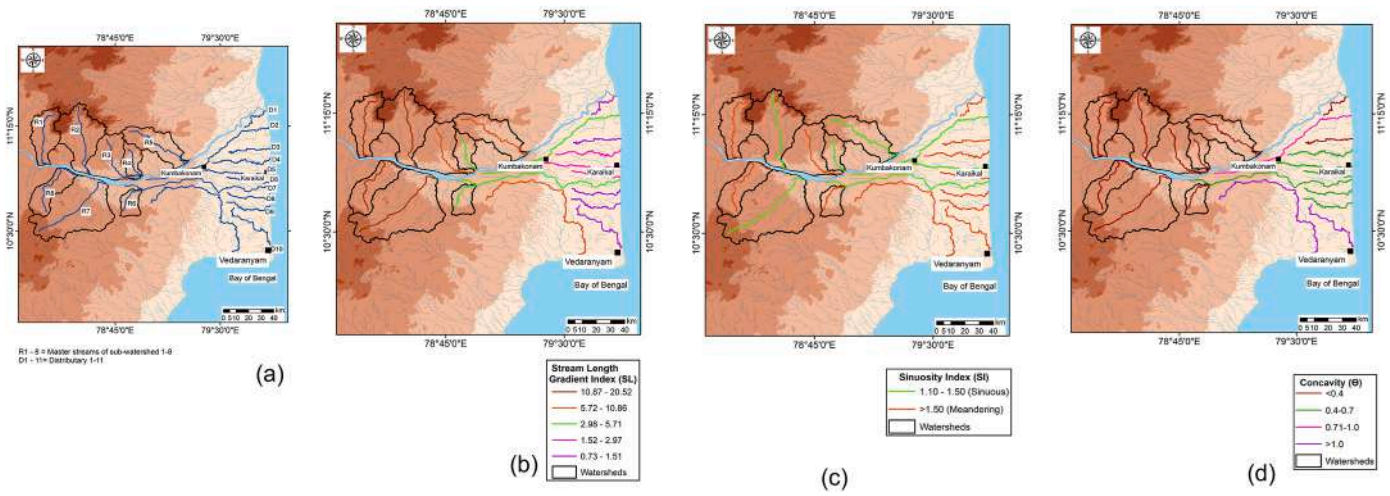

Fig. 3. a. The master streams of the selected sub-watersheds and distributaries of the Cauvery delta region. **b.** Stream length gradient index (SL) of the master streams of eight sub-watersheds and main distributaries of the Cauvery delta region. **c.** Sinuosity index (SI) of the master streams of eight sub-watersheds and main distributaries of the Cauvery delta region. **d.** Channel Concavity (Θ) of the master streams of eight sub-watersheds and main distributaries of the Cauvery delta region.

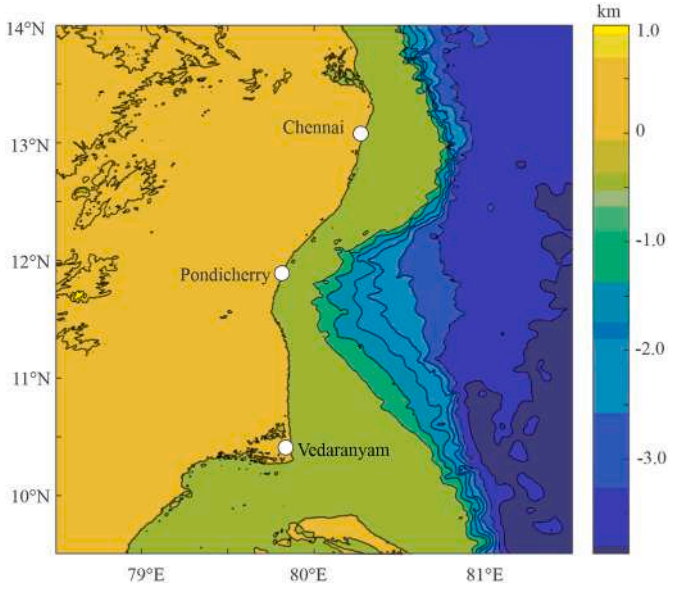

Fig. 4. Regional map of Cauvery basin has been plotted by using the GEBCO bathymetry data. Coluor bar: height in km with respect to the mean sea level (MSL).

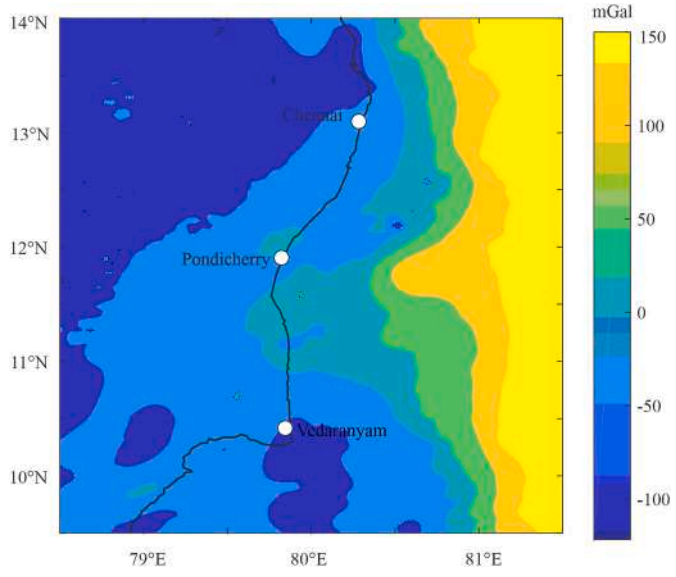

Fig. 5. Effect of gravity on uncompensated bathymetry topographic height in the Cauvery basin.

(AF = 15.562) is found in the sub-watershed 6, which has a westward tilt. Sub-watersheds 3 and 8 exhibit greater asymmetry, with AF = 10.567 and 14.711, respectively. With the lowest AF = 0.252, Watershed 2 is least tilted and is the most symmetric river basin. The values of Elongation Ratio (Re) represent the lateral expansion of the watersheds and their steady evolution. With Re = 0.579, Watershed 5 has the longest form. This watershed's Circularity Ratio (Rc) = 0.284 also indicates that it underwent the least amount of lateral expansion. With Re = 0.852, sub-watershed 3 at the left bank of the Cauvery River has the maximum lateral expansion. With Rc = 0.383, sub-watersheds 4 and 6 have maximum circularity. The Basin Shape Index (Bs), which is minimum (1.396) for sub-watershed 2 and maximum (3.429) for the sub-watershed 8, further supports the elongated character of those sub-watersheds. The Transverse Topographic Symmetry Factor (T) indicates how each sub-watershed's master streams deviate from their mid-path due to tilting. Sub-watershed 6's T = 0.830 indicates that the master stream's greatest tilting. For sub-watershed 7, the lowest value of T = 0.150 is indicated. For sub-watershed 1, the drainage texture (Dt) is maximum (0.861). Additionally, sub-watershed 7 exhibits a higher value of Dt = 0.874. The Dt's minimum value of 0.304 is found for the sub-watershed 4.

3.1.2. Clustering

The dendrogram created using the squared Euclidian distance method based on the calculated values of the parameters allowed clustering for all the watersheds (Fig. 2). Comparing groups of comparable waterway profiles among varied settings is possible through cluster analysis of waterway profiles. A symmetric nearness lattice is constructed using the computed dR values (Table 3). According to the rescaled remove cluster combination, there is just one major cluster consisting of sub-watersheds 1, 2 and 5.

3.1.3. Linear parameters

The linear parameters applied on the selected rivers show significant variation (Fig. 3a). The stream length gradient index (SL) is portrayed in five distinct classes-class 1 (10.87–20.52), class 2 (5.75–10.86), class 3

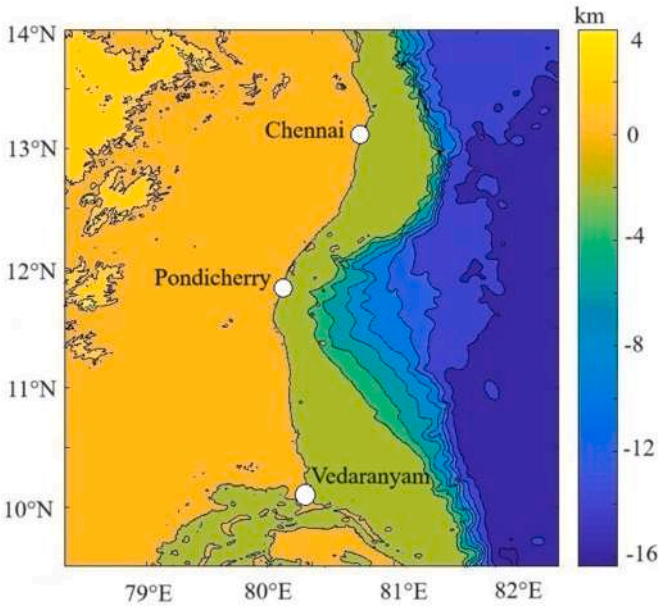

Fig. 6. Regional Free Air Gravity (FAG) anomaly map of Cauvery basin. Colour bar: gravity tend (mGal).

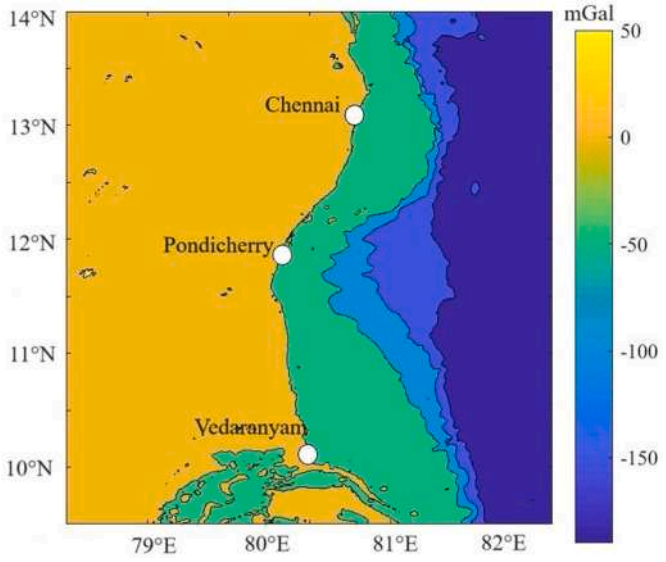

Fig. 7. The interface of crust and mantle map of Cauvery basin based on GEBCO bathymetry data. Colour bar: height and depth with respect to the mean sea level (MSL).

(2.98–5.71), class 4 (1.52–2.97) and class 5 (0.73–1.51) (Fig. 3b). Master streams of sub-watersheds 1, 2, 7 and 8 fall under class 1. Most of the distributaries in the delta region exhibit very less gradient and come under class 4 and 5.

The sinuosity index (SI) does not portray much variation among the considered master streams and distributaries. The master streams of sub-watershed 2, 4, 5 and 7 are sinuous. Among the distributaries, watersheds 2, 5 and 7 have SI = 1.10–1.50 (Fig. 3c).

It is interesting to note that all the master steam of the selected sub-watersheds (1–8) have $\Theta < 0.4$. (Fig. 3d).

3.2. Geophysical aspect

We selected h(x,y) from the bathymetric height (here depth)

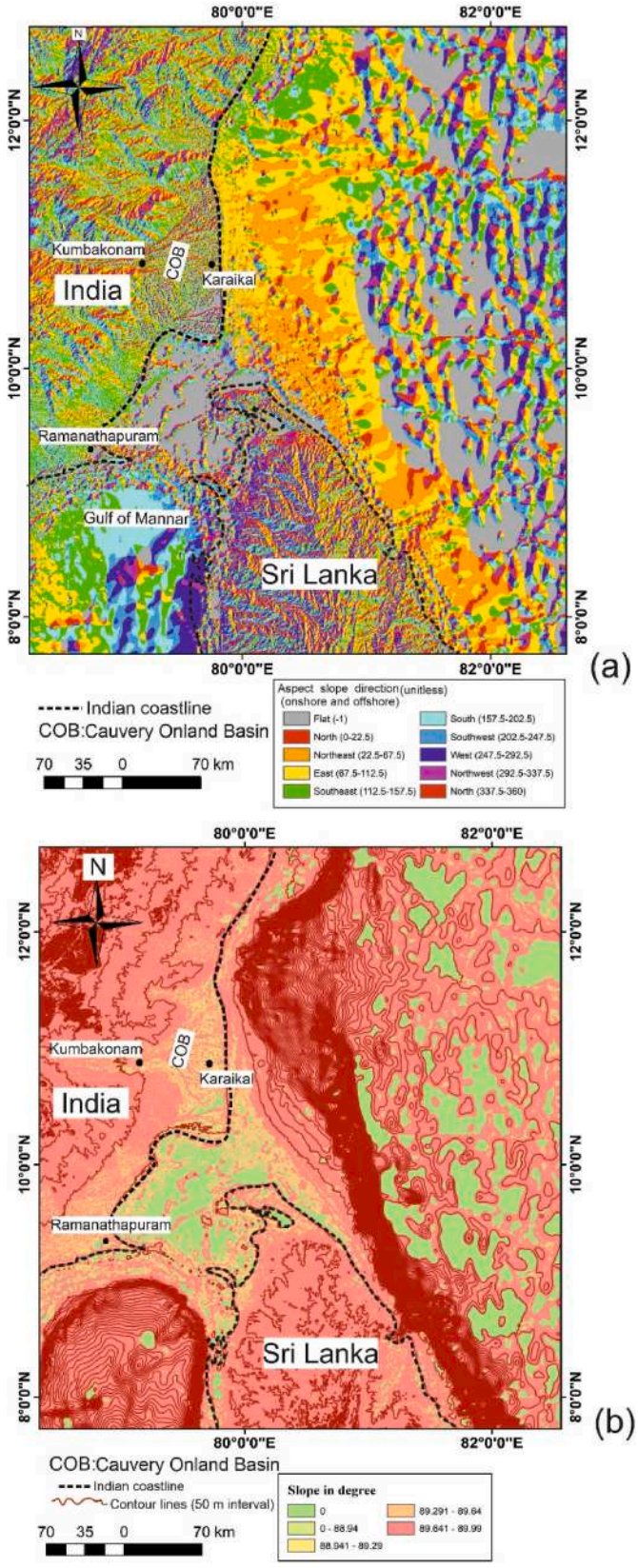

Fig. 8. a. Slope direction map based on under marine DEM data. Ten slope directions are mapped both on land and bottom sea topography. **b.** Contour mapping at 50 m interval of both land and under marine regions with slope amounts in degrees.

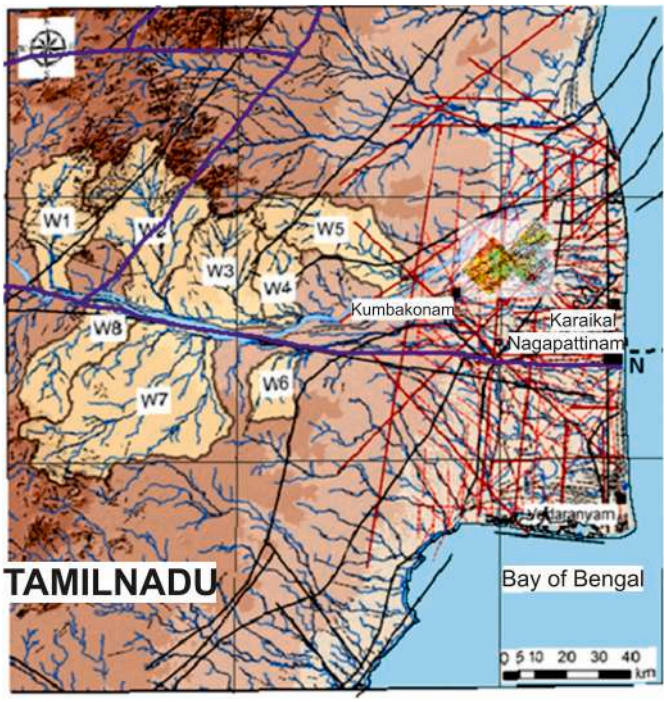

Fig. 9. Lineaments near Karikal-Nagapattinam (on-shore) area trends ~ E-W and correlate with the Cauvery Shear Zone (Chetty, 2015) in the west. Faults in the offshore region marked based on magnetic data (Subhramanyam et al., 1995) are also continuation of the on-shore trends. ArcGIS 10.5 was used to overlay and correlate different relevant geo-spatial datasets for analysis and pattern recognition.

(GEBCO) and estimated the gravity effect of the uncompensated bathymetry (Figs. 4 and 5). The densities of crust (ρ_c) and mantle (ρ_m) are taken as 2.67 g cm^{-3} and 3.3 g cm^{-3}, respectively (Ganguli and Pal, 2023). In the current study, we selected d = 42 km and k = 0.04 km^{-1} (Ussami et al., 1993). The gravity anomaly varies regionally from 50 to −150 mGal. A gravity anomaly map is created covering the onshore and offshore areas of the Cauvery basin (Fig. 6) by taking the free-air gravity (FAG) data from the International Gravimetric Bureau (Internet ref-2). There are various gravity low and high values, which might be related to the seismically mapped basement ridge-depression features (Twinkle et al., 2014). The map showed the large negative anomalies up to −140 mGal of the Indian shield crustal part in the west (Fig. 6). The shelf edge gravity anomalies in the offshore region between Pondicherry and Vedaranyam can be clearly seen with two prominent gravity lows of around −100 mGal separated by high magnitude (~20 mGal) anomalies. This kind of anomaly orientation indicates the extension of the sub-basin in the region. The map shows a strong NE-SW gravity trend (Fig. 6), which possibly indicates a high-density plug at mid-crust. The low values of gravity near the Vedaranyam region indicates low density rocks within the basement (Ganguli and Pal, 2023).

The H(x,y) value is chosen as 34 km (Ganguli and Pal, 2023). Eqn (3) indicates that only the term h(x,y) varies and other terms are constants, hence the local isostatic compensation map (Fig. 7) resembles Fig. 1. The variation of this compensation is +4 km in the crustal part, around −4 km in the coastal part, and it further lowers to around −16 km at the eastern part at greater depths of the sea.

3.3. Bathymetric aspect

Slope direction map in terms of the aspect slope map (Fig. 8a) shows NE and E directions. However, it is predictable that the ridges are made up of multi-slope directions. Based on flat topography, multi-directional ridges are prominent in the offshore areas. Slope amount varies widely. Flat topography possibly indicates the depressed land. The contours at 50 m interval disclose the slope patter as the closely-spaced contours define the area to be steeply sloped towards the sea. Patches of contours on the sea floor determine the ridges with multidirectional slope (Fig. 8b). As per the DEM-based contour mapping along the Cauvery delta towards the east and south-east, slope change to moderate to steep. From the coast line, there may be a sudden steep slope near the continental slope and further towards the sea.

4. Discussions

4.1. Morphology & link with tectonics

We performed geomorphologic analysis from the southern part of the Cauvery basin's onland area. Previous authors commented that this southern portion is tectonically less active than the northern portion of the onland part of the Cauvery basin. The values of AF for different (sub) watersheds suggest that tilting of the sub-watersheds owing to tectonic imprint is insignificant. This is also supported by the magnitudes of Transverse Topographic Symmetry Factor. The Stream Length Gradient Index for the main channels as well as the distributaries suggest gentler gradient, which might be attributed to the flat rolling topography of the study area.

An analysis of the overall lineament pattern (Fig. 9) shows a dominance of an E-W trend around the Nagapattinam region. A spatial correlation between these lineament trends with the magnetic lineaments in the offshore region indicates that these E-W lineament trends extend further westwards at least up to the Continental Ocean Boundary (COB). These E-W trends are also found to broadly correlate with the lower course of the Cauvery river and can be attributed to the manifestation of the Cauvery Shear Zone.

The E-W trend also match with the strike of the faults that we delineate atop the Precambrian basement in the Kuthalam area based on the 3D seismic data (Fig. 10a). A coherency time-slice in the same area approximately conforming to the top of the Precambrian basement suggesting discontinuities reveal sheath folds with ~ E-W trending fold axis associated with a dextral strike slip (Fig. 10b). Such folds form due to profound drag parallel to the simple shear (review in Mukherjee et al., 2015) and can be observable in outcrops in different scales (Fig. 10c). The E-W trend is also prominently depicted in a Residual Gravity map (KDMIPE, 2017) implying a deeper crustal control and appears to be a continuation of the faults marked by seismic data and lineaments from geomorphic data (Fig. 10d).

4.2. Geophysics

The Cauvery basin topographic map has been generated by the General Bathymetric Chart of the Oceans (GEBCO) bathymetry data (Internet ref-1) and plotted in the MATLAB 2017 environment (Fig. 1). The offshore area is characterized by an elevation of <1 km and reaching up to around - 4 km. This kind of depth variation indicates the presence of sub-basins. The shelf widens from Pondicherry to the north of Chennai. The shelf narrows from south of Pondicherry up to Vedaranyam. Bathymetric has been studied by several researchers and a submarine canyon in the Pondicherry region has been deciphered (Varadachari et al., 1968; Bastia et al., 2011; Twinkle et al., 2014). They used techniques such as horizontal gradient (HG), first vertical derivative (FVD) and second vertical derivative (SVD) are used in order to resolve and identify geological features, which include faults, basements, edge of geological features and gravity trends. Rao et al. (1992) found major valleys/mega lineaments near Pondicherry. Lineaments have significant roles in shaping the shelf-slope morphology, besides the other geologic processes (Murthy et al., 2012).

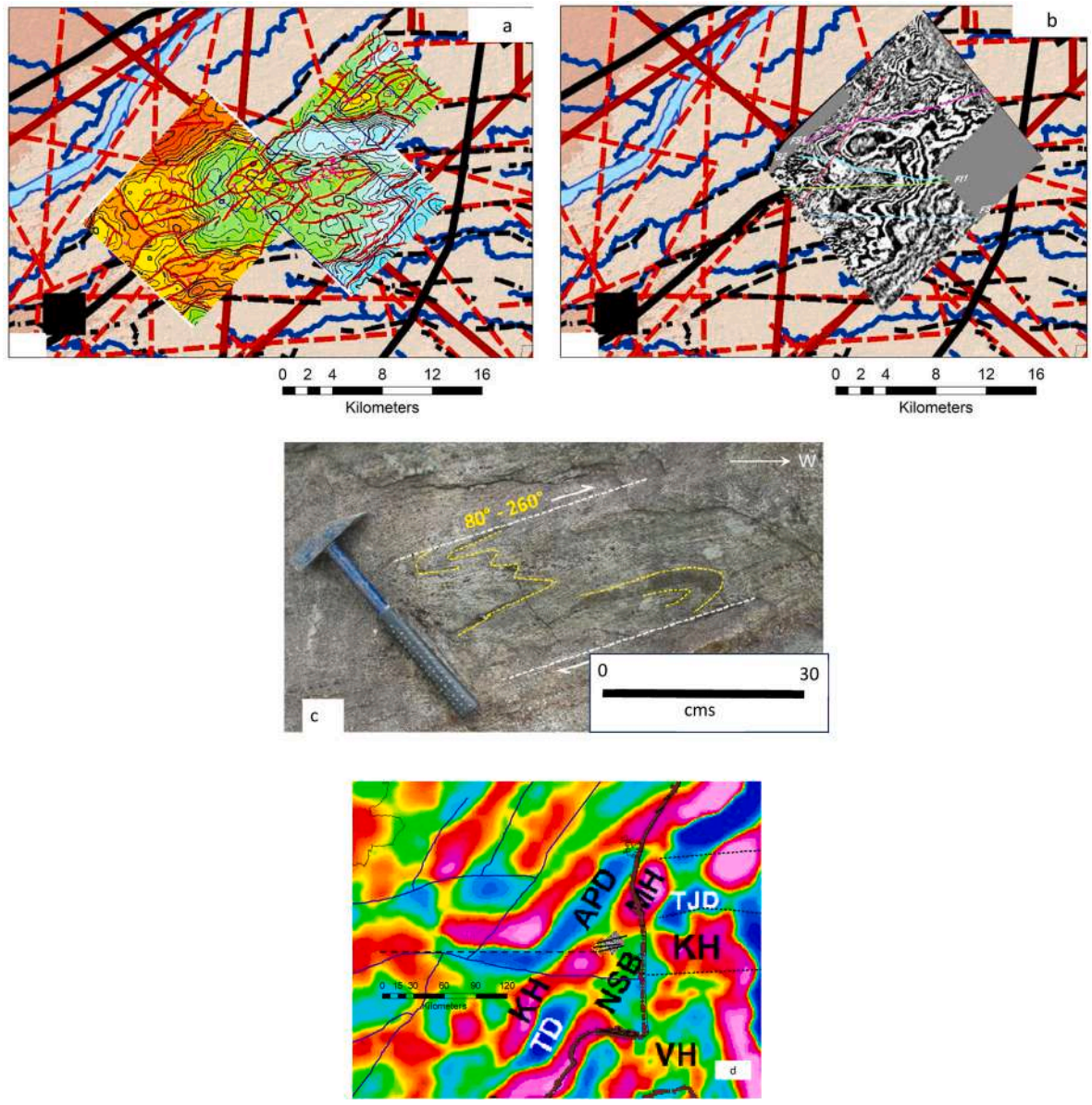

Fig. 10. ab. Faults (depicted as bold red lines) marked atop the basement based on 3D seismic data (Mazumder et al., 2015) correlating with lineaments. Location of the figure is presented in Fig. 9. A time slice at ~2000 ms time equivalent depth. corresponding to Precambrian basement top plausibly indicates development of sheath fold associated with E-W faults (Mazumder et al., 2015). **c.** Sheath folds as observed on a horizontal section in Neoproterozoic mylonites in the Salem area (Tamil Nadu) where the Cauvery shear zone is exposed. **d.** A prominent E-W trend is observed in the residual gravity map (KDMIPE, 2017) that correlates with faults marked from seismic data and geomorphic lineaments. Warmer or reddish-yellowish colours denote gravity highs whereas cooler or bluish-greenish colours gravity lows, which broadly correspond to highs and depressions created during Lower Cretaceous rifting of India-Antarctica. APD: Ariyalur-Pondicherry Depression, KH: Karaikal High, MH: Madanam High, TD: Tranquebar Depression, TJD: Thanjavur Depression. VH: Vedarniyam High.

5. Conclusions

The morphometric analysis of the study area reveals different degrees of tectonics on the selected (sub)watersheds. Watersheds 1, 2 and 5 come under the same cluster, which indicates that for the selected morphometric parameters these (sub)watersheds behave similarly. The main channels of the selected (sub)watersheds portrays greater SL values (10.87–20.52) than the distributaries. The flat terrain has resulted in the lesser (0.73–1.51) SL values of the distributaries. The distributaries finally meet the Bay of Bengal following a straight path contributing to the lesser SI values (1.10–1.50). The Cauvery basin topographic map generated by the GEBCO bathymetry data is characterized by an elevation of <1 km up to - 4 km. The gravity anomaly in the same region varies regionally from 50 to −150 mGal while in the offshore region between Pondicherry and Vedaranyam gravity values are ~ −100 mGal separated by higher magnitude (~20 mGal) anomalies. The gravity values are low (−100 mGal) near the Vedaranyam region because of presumably low-density rocks within the basement. Airy-Heiskanen model is used to analyze the local isostatic study within the region. The results indicate that the variation of local isostatic compensation is +4 km in the crustal part, around −4 km in the coastal part, and it further lowers to around −16 km in the eastern part at greater depths of the sea. Bathymetric studies revealed multidirectional slopes. Relatively flat areas in the offshore areas can be depocenters. The mapped E-W linear trends of lineaments appear to be manifestations of Cauvery Shear zone that also continue offshore and appear to be deep seated crustal elements.

Software used in this work

ArcGIS 10.4.
ArcGIS 10.5.
IBM SPSS Statistics 26.
MATLAB (Ver: 2017b)

CRediT authorship contribution statement

Soumyajit Mukherjee: Writing – review & editing, Writing – original draft, Conceptualization. **Kutubuddin Ansari:** Writing – original draft, Formal analysis. **Adrija Raha:** Investigation, Formal analysis. **Mery Biswas:** Writing – original draft, Formal analysis. **Subhobroto Mazumder:** Investigation.

Declaration of competing interest

The authors declare that they have no known competing financial interests or personal relationships that could have appeared to influence the work reported in this paper.

Data availability

Data will be made available on request.

Acknowledgements

Self-funded work. The Associate Editor and the two reviewers are thanked for providing comments that helped to clarify several points.

Abbreviations & symbols

AF	Asymmetry Factor
APD	Ariyalur-Pondicherry Depression
Bs	Basin Shape Index
DMB	Digital Bathymetric Model
Dt	Drainage Texture
ECMI	Eastern Continental Margin of India
FAG	Free-Air Gravity
FVD	First Vertical Derivative
GEBCO	General Bathymetric Chart of the Oceans
GIS	Geographical Information system
HG	Horizontal Gradient
KH	Karaikal High
MH	Madanam High
MSL	Mean Sea Level
Rc	Circularity Ratio
Re	Elongation Ratio
SI	Sinuosity Index
SL	Stream length Gradient Index
SVD	Second Vertical Derivative
T	Transverse Topographic Symmetry Factor
TD	Tranquebar Depression
TJD	Thanjavur Depression
USA	United States of America
VH	Vedarniyam High
Θ	Concavity Index

References

Agarwal, R.P., Mitra, D., 1991. Geomorphology of Cauvery basin Tamil Nadu, based on interpretation of Indian Remote sensing Satellite (IRS) data. Journal of the Indian Society of Remote Sensing 19, 263–267.
Anand, A.K., Pradhan, S.P., 2019. Assessment of active tectonics from geomorphic indices and morphometric parameters in part of Ganga basin. J. Mt. Sci. 16, 1943–1961.
Bastia, R., Radhakrishna, M., 2012. Basin Evolution and Petroleum Prospectivity of the Continental Margins of India. Elsevier.
Bastia, R., Radhakrishna, M., Nayak, S., 2011. Identification and characterization of marine geohazards in the deep water eastern offshore of India: constraints from multibeam bathymetry, side scan sonar and 3D high-resolution seismic data. Nat. Hazards 57, 107–120.
Bishop, P., Young, R.W., McDougall, I., 1985. Stream profile change and long-term landscape evolution: early miocene and modern rivers of the east Australian highland crest, central new south wales, Australia. J. Geol. 93, 455–474.
Biswas M, Ansari K, Raha A, Shilpashree ML, Mukherjee S. Submitted. Morphometry, gravity analyses and active tectonics of the Gulf of Mannar in the Indian sector. Evolving Earth.
Biswas, M., Puniya, M.K., Gogoi, M.P., Dasgupta, S., Mukherjee, S., Kar, N.R., 2022. Morphotectonic analysis of petroliferous Barmer rift basin (Rajasthan, India). J. Earth Syst. Sci. 131, 140.
Born, G.H., Dunne, J.A., Lame, D.B., 1979. Seasat mission overview. Science 204 (4400), 1405–1406.
Bull, W.B., McFadden, L.D., 1977. Tectonic geomorphology north and south of the garlock fault, California. Proceedings of the eighth annual geomorphology symposium. In: Doehring, D.O. (Ed.), Geomorphology in Arid Regions. State University of New York, Binghamton, pp. 115–138.
Chetty, T.R.K., 2015. The Cauvery suture zone: map of structural architecture and recent advances. J. Geol. Soc. India 85, 37–44.
Chetty, T.R.K., Rao, Y.B., 2006. The Cauvery shear zone, Southern Granulite Terrain, India: a crustal-scale flower structure. Gondwana Res. 10, 77–85.
Cox RT, 1994. Analysis of drainage-basin symmetry as a rapid technique to identify areas of possible Quaternary tilt-block tectonics: an example from the Mississippi Embayment. Geol. Soc. Am. Bull. 106, 571–581.
Dasgupta, S., 2018. Pull-apart basin in the offshore cauvery–palar basin, India. In: Misra, A.A., Mukherjee, S. (Eds.), Atlas of Structural Geological Interpretation from Seismic Images. Wiley Blackwell, pp. 127–129.
Dasgupta, S., 2019. Implication of transfer zones in rift fault propagation: example from Cauvery basin, Indian east coast. In: Mukherjee, S. (Ed.), Tectonics and Structural Geology: Indian Context. Springer, pp. 313–326. ISBN: 978-3-319-99340-9.
Dasgupta, S., Maitra, A., 2018. Transfer zone geometry in the offshore Cauvery Basin, India. In: Misra, A.A., Mukherjee, S. (Eds.), Atlas of Structural Geological Interpretation from Seismic Images. Wiley Blackwell, pp. 117–121.
Dasgupta, S., Misra, A.A., 2018. Polygonal fault system in late cretaceous sediments of Cauvery deepwater Basin, India. In: Misra, A.A., Mukherjee, S. (Eds.), Atlas of Structural Geological Interpretation from Seismic Images. Wiley Blackwell, pp. 113–116.
Dasgupta, S., Biswas, M., Mukherjee, S., Chatterjee, R., 2022. Structural evolution and sediment depositional system along the transform margin- Palar–Pennar basin, Indian east coast. J. Pet. Sci. Eng. 211, 110155.
Deepa, Nagaraju, J., Chetia, B., Tandon, R., Chaudhuary, P.K., Bhardwaj, A., 2019. Integrated study of a fractured granitic basement reservoir with connectivity analysis and identification of sweet spots: Cauvery Basin, India. Lead. Edge 38, 254–261.
Ganguli, S.S., Pal, S.K., 2023. Gravity-magnetic appraisal of the southern part of Cauvery Basin, Eastern Continental Margin of India (ECMI); an evidence of volcanic rifted margin. Front. Earth Sci. 11, 1190106.
Goldrick, G., Bishop, P., 1995. Differentiating the roles of lithology and uplift in the steepening of bedrock river long profiles. J. Geol. 103, 227–231.
Goldrick, G., Bishop, P., 2007. Regional analysis of bedrock stream long profiles: evaluation of Hack's SL form, and formulation and assessment of an alternative (the DS Form). Earth Surf. Process. Landforms 32, 649–671.
Hack, J.T., 1957. Studies of Longitudinal Stream Profile in Virginia and Maryland. US Geological Survey Professional Paper 294-B, pp. 45–95.
Hare, P.W., Gardner, T.W., 1985. Geomorphic indicators of vertical neotectonism along converging plate margins, Nicoya Peninsula. Costa Rica. Binghamton Symposia in Geomorphology: International Series 15, 75–104.
Hell, B., 2011. Mapping Bathymetry: from Measurement to Applications (Doctoral Dissertation. Department of Geological Sciences, Stockholm University. ISBN 978-91-7447-309-4.
Horton, R.E., 1945. Erosional development of streams and their drainage basins: hydrophysical approach to quantitative morphology. GSA Bulletin 56, 275–370.
Internet ref 1:https://download.gebco.net/(Accessed on 12-December-2023).
Internet ref 2:https://www.gebco.net/data_and_products/gridded_bathymetry_data/#global (Accessed on 12-December-2023).
Internet ref-3:URL: http:/www.gebco.net/data_and_products (Accessed on 12-July-2023).
Internet ref-4:URL: https://bgi.obs-mip.fr/data-products/outils/egm2008-anomaly-maps-visualization/(Accessed on 13-July-2023).
KDMIPE, 2017. Residual gravity anomaly atlas of Indian sedimentary basins. Oil and Natural Gas Corporation.
Klenke, M., Schinke, H.W., 2002. A new bathymetric model for the central Fram Strait. Mar. Geophys. Res. 23, 367–378.
Kumar, N., Singh, A.P., Singh, B., 2011. Insights into the crustal structure and geodynamic evolution of the southern granulite terrain, India, from isostatic considerations. Pure Appl. Geophys. 168, 1781–1798.
Lee, C.S., Tsai, L.L., 2009. A quantitative analysis for geomorphic indices of longitudinal river profile: a case-study of the Choushui River, Central Taiwan. Environ. Earth Sci. 59, 1549–1558.
Leopold, L.B., Wolman, M.G., 1960. River meanders. Geol. Soc. Am. Bull. 71, 769–793.
Mazumder, S., Tep, B., Pangtey, K.K.S., 2015. A Remote Sensing and GIS Based Integrated Approach for Identifying Promising Areas for Basement Exploration in

Cauvery Basin. 11th Biennial International Conference & Exposition of Geophysics, SPG Jaipur.
Mazumder, S., Tep, B., Pangtey, K.K.S., Mitra, D.S., 2019. Basement tectonics and shear zones in Cauvery Basin (India): implications in hydrocarbon exploration. In: Mukherjee, S. (Ed.), Tectonics and Structural Geology: Indian Context. Springer, pp. 279–311.
Misra, A.A., Dasgupta, S., 2018a. Transform margin in the Cauvery Basin, Indian east coast passive margin. In: Misra, A.A., Mukherjee, S. (Eds.), Atlas of Structural Geological Interpretation from Seismic Images. Wiley Blackwell, pp. 235–239.
Misra, A.A., Dasgupta, S., 2018b. Shallow detachment along a transform margin in Cauvery Basin, India. In: Misra, A.A., Mukherjee, S. (Eds.), Atlas of Structural Geological Interpretation from Seismic Images. Wiley Blackwell, pp. 101–105.
Mogali, P., Singh, A., Desai, B.G., 2024. Unlocking the hidden potential: petrophysical analysis of adjoining basement reservoirs in the Cauvery Basin's Madanam Palaeo-High. J. Earth Syst. Sci. 133, 1–20.
Mondal, B., Biswas, M., Mukherjee, S., Shaikh, M.A., 2023. Geomorphic signatures and active tectonics in western Saurashtra, Gujarat, India. J. Geodesy Geodyn. 15, 82–99.
Mukherjee, S., Punekar, J., Mahadani, T., Mukherjee, R., 2015. A review on intrafolial folds and their morphologies from the detachments of the western Indian Higher Himalaya. In: Mukherjee, S., Mulchrone, K.F. (Eds.), Ductile Shear Zones: from Micro- to Macro-Scales. Wiley Blackwell, pp. 182–205.
Murthy, K.S.R., Subrahmanyam, A.S., Subrahmanyam, V., 2012. Tectonics of the Eastern Continental Margin of India. The Energy and Resources Institute (TERI).
Parker, R.L., 1973. The rapid calculation of potential anomalies. Geophys. J. Int. 31, 447–455.
Pasari, S., Simanjuntak, A.V.H., Mehta, A., et al., 2021. The current state of earthquake potential on java island, Indonesia. Pure Appl. Geophys. 178, 2789–2806.
Raha, A., Biswas, M., Mukherjee, S., 2023. Application of Topsis model in active tectonic prioritization: madeira watershed, South America. J. S. Am. Earth Sci. 129, 104502.
Ramasamy, S.M., Saravanavel, J., 2020. Remote Sensing revealed geomorphic anomalies and recent earth movements in Cauvery delta, Tamil Nadu, India. Journal of the Indian Society of Remote Sensing 48, 1809–1827.
Ramasamy, S.M., Kumanan, C.J., Selvakumar, R., Saravanavel, J., 2011. Remote sensing revealed drainage anomalies and related tectonics of South India. Tectonophysics 501, 41–51.
Ramírez-Herrera, M.T., 1998. Geomorphic assessment of active tectonics in the Acambay graben, Mexican volcanic belt. Earth Surf. Process. Landforms 23, 317–332.
Ramkumar, M., et al., 2019. Tectono-morphological evolution of the Cauvery, Vaigai, and Thamirabarani River basins: implications on timing, stratigraphic markers, relative roles of intrinsic and extrinsic factors, and transience of Southern Indian landscape. Geol. J. 54, 2870–2911.
Rao, L.H.J., Rao, T.S., Reddy, D.R.S., Biswas, N.R., Mohapatra, G.P., Murty, P.S.N., 1992. Morphology and sedimentation of continental slope, rise and abyssal plain of western part of Bay of Bengal. Visesa Prakasana-Bharatiya Bhuvaijñanika Sarveksana 29, 209–217.
Saha, S.K., 2022. Remote sensing and geographic information system applications in hydrocarbon exploration: a review. Journal of the Indian Society of Remote Sensing 50, 1457–1475.
Schumm, S.A., 1956. Evolution of drainage systems and slopes in badlands at Perth Amboy, New Jersey. Bull. Geol. Soc. Am. 67, 597–646.
Seeber, L., Gornitz, V., 1983. River profiles along the Himalayan arc as indicators of active tectonics. Tectonophysics 92, 335–367.
Sharma, A., Rajamani, V., 2000. Weathering of gneissic rocks in the upper reaches of Cauvery river, south India: implications to neotectonics of the region. Chem. Geol. 166, 203–223.
Simanjuntak, A.V.H., Palgunadi, K.H., Supendi, P., 2024. The western extension of the Balantak Fault revealed by the 2021 earthquake cascade in the central arm of Sulawesi, Indonesia. Geosci. Lett. 11, 35.
Twinkle, D., Rao, G.S., Radhakrishna, M., Murthy, K.S.R., 2016. Crustal structure and rift tectonics across the Cauvery–Palar basin, Eastern Continental Margin of India based on seismic and potential field modelling. J. Earth Syst. Sci. 125, 329–342.
Ussami, N., de Sá, N.C., Molina, E.C., 1993. Gravity map of Brazil: 2. Regional and residual isostatic anomalies and their correlation with major tectonic provinces. J. Geophys. Res. Solid Earth 98, 2199–2208.
Varadachari, V.V.R., Nair, R.R., Murty, P.S.N., 1968. Submarine canyons off the Coromandel coast. Bull. Natl. Inst. Sci. India 38, 457–462.
Watts, A.B., 2001. Isostasy and Flexure of the Lithosphere. Cambridge University Press.
Wołosiewicz, B., 2018. The influence of the deep seated geological structures on the landscape morphology of the Dunajec River catchment area, Central Carpathians, Poland and Slovakia. Geosci. J. 7, 21–47.
Zou, C., 2017. Unconventional Petroleum Geology. Elsevier.